Structure of tellurite glasses—effects of K_2O or P_2O_5 additions studied by diffraction

2005 J. Phys.: Condens. Matter 17 2365

(http://iopscience.iop.org/0953-8984/17/15/009)

INSTITUTE OF PHYSICS PUBLISHING JOURNAL OF PHYSICS: CONDENSED MATTER

J. Phys.: Condens. Matter **17** (2005) 2365–2386 doi:10.1088/0953-8984/17/15/009

Structure of tellurite glasses—effects of K_2O or P_2O_5 additions studied by diffraction

U Hoppe[1], I Gugov[2,3], H Bürger[2], P Jóvári[4,5] and A C Hannon[6]

[1] Institute for Physics, Rostock University, Rostock D-18051, Germany
[2] Otto Schott Institute for Glass Chemistry, Friedrich Schiller University Jena, Jena D-07743, Germany
[3] Department of Physics, University of Chemical Technology and Metallurgy, Sofia 1756, Bulgaria
[4] Hamburger Synchrotronstrahlungslabor (HASYLAB) am Deutschen Elektronen-Synchrotron (DESY), Notkestraße 85, Hamburg D-22607, Germany
[5] Research Institute for Solid State Physics and Optics, Hungarian Academy of Sciences, POB 49, Budapest H-1525, Hungary
[6] ISIS Facility, Rutherford Appleton Laboratory, Chilton, Didcot OX11 0QX, UK

Received 20 January 2005, in final form 10 March 2005
Published 1 April 2005
Online at stacks.iop.org/JPhysCM/17/2365

Abstract

Neutron and x-ray diffraction experiments of high resolving power with neutrons from a spallation source and high-energy photons from a synchrotron have been performed on compositional series of binary tellurite glasses with additions of K_2O or P_2O_5 (max. 16 or 32 mol%). Since the P–O bond lengths do not interfere with the Te–O peaks the Te–O and O–O correlations are approximated by Gaussian fitting of the x-ray and neutron correlation functions up to lengths of 0.28 nm. In the case of K_2O–TeO_2 glasses reasonable assumptions are made for the K–O first-neighbour peaks. Te–O and O–O coordination numbers are four and five for the glasses of compositions close to pure TeO_2 which indicates formation of a three-dimensional network of corner-connected TeO_4 trigonal bipyramids. The tellurite network groups are TeO_4 and TeO_3 units in K_2O–TeO_2 glasses and TeO_4 and TeO_5 units in P_2O_5–TeO_2 glasses. Additional Te–O neighbours found at 0.23 nm $< r <$ 0.26 nm for K_2O–TeO_2 glasses suggest the existence of TeO_{3+1} units and those found at 0.23 nm $< r <$ 0.29 nm for the P_2O_5–TeO_2 glasses indicate the existence of distorted TeO_6 polyhedra. Tellurite networks are flexible to form the appropriate coordination environments for quite different ions or groups of opposite charge such as K^+ ions and $(PO_{4/2})^-$ tetrahedra where change of the TeO_n network units provides the needed number of oxygen neighbours.

1. Introduction

Tellurite glasses are attracting a lot of attention because of their high refractive index (see e.g. [1] and the literature therein), anomalous partial dispersion in the visible light region [2], high acousto-optical figure of merit [3], high third-order non-linear susceptibility [4, 5], good lasing [6] and optical amplifying properties [7], as well as good transmittance in the near-infrared region (NIR) [8]. In some specific cases these properties are combined with good chemical and crystallization stability [9].

The main peculiarity of the structure of tellurite crystals, melts and glasses is the presence of a sterically active lone pair of the $5s^2$ electrons (LPE) at the tellurium(IV) atom. For example, the LPE causes an enormous variability of the Te–O bond lengths in tellurite crystals [10, 11]. Actually, it is often difficult to separate the oxygen atoms in tellurite structures into the classical bridging and non-bridging types only. Intermediate oxygen atoms, called semi-bridging [12], can be found in these structures too. Another characteristic is the temperature-induced, charge-independent change of the Te–O coordination number in tellurite melts [13] which causes a fast depolymerization of their network on heating and which predetermines their 'fragility' [14]. The structural variability of tellurite materials could be used to tailor the physical properties of glasses as well as their thermal and chemical stability parameters. This possibility justifies the steady interest in structural investigations of tellurite glasses.

The aim of the present contribution is to study the short-range order (SRO) of binary tellurite glasses using x-ray and neutron diffraction techniques. The oxides K_2O and P_2O_5 are chosen as second components of the glasses because K_2O is a typical network modifier (or Lewis base), but P_2O_5 represents a typical network former (or Lewis acid). Both systems, K_2O–TeO_2 and P_2O_5–TeO_2, possess relatively large glass-forming regions [15]. Moreover, the Te–O, K–O and P–O distances differ clearly, which simplifies the structural evaluations. The K_2O–TeO_2 system is widely studied with diffraction [16–18] and spectroscopic [18–22] methods. But not much is known about the structural behaviour in the P_2O_5–TeO_2 system. Some diffraction work was performed on tellurite glasses of small P_2O_5 content [23].

2. Experimental details

Three samples of the K_2O–TeO_2 system and six samples of the P_2O_5–TeO_2 system were prepared with compositions listed in table 1. The glasses were melted in covered gold crucibles for 1.5 h at 800 °C for the K_2O–TeO_2 samples and at 850–900 °C for the P_2O_5–TeO_2 samples. The melts were cast into cold brass moulds. The glasses were annealed at 300 °C and, subsequently, cooled down slowly. The sample with 2 mol% P_2O_5 was pressed on a cold copper block to avoid crystallization. Mass densities were measured by Archimedes' principle. Nominal compositions were used for the structural analysis. Densities and compositions are given in table 1. From the area of the P–O peaks with coordination numbers, N_{PO}, of ∼3.5 (four is expected) it reveals that the real P_2O_5 contents of the P_2O_5–TeO_2 glasses were reduced during melting (cf section 3.4). The final P_2O_5 fractions are also given in table 1. The new compositions were chosen to fit with numbers N_{PO} of four. Also the sums of bond valencies were checked for the different Te–O distances of the Te(IV) atoms to give reasonable numbers (cf section 3.3).

The neutron diffraction experiments were performed at the GEM diffractometer of the spallation source ISIS of the Rutherford Appleton Laboratory (Chilton/UK). The glassy material was crushed and loaded into vanadium cylinders 8.3 mm in diameter and with wall thickness of only 0.025 mm. The beam size was 12×40 mm^2. The duration of the data collection was at least 3 h for each sample. A 6 mm vanadium rod was used to obtain the

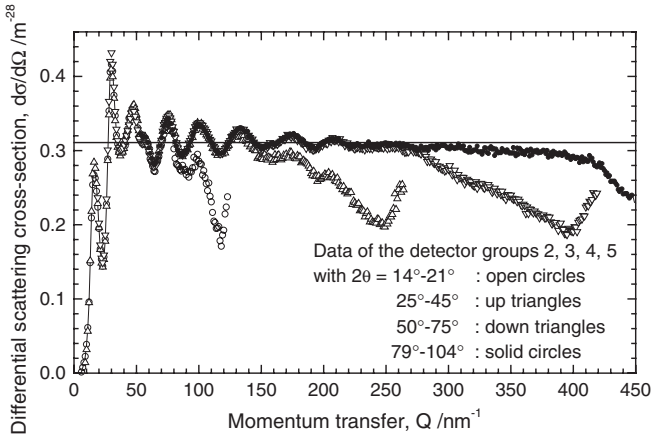

Figure 1. Differential scattering cross-sections, $d\sigma/d\Omega$, of sample tep14 obtained by neutron diffraction. The data shown of four detector groups of the GEM instrument result after finishing all corrections and normalization. These data are used to obtain the final structure factor.

Table 1. Compositions and densities of the tellurite glasses studied. Glasses with K_2O are named tek; those with P_2O_5 are given labels tep.

Sample label	K_2O or P_2O_5 content			Mass density	Number density
	As badged	Corrected	$c(M_zO)$	(g cm^{-3})	of atoms (nm^{-3})
tek08	0.08	—	0.080	5.083(2)	59.49
tek12	0.12	—	0.120	4.850(2)	57.74
tek16	0.16	—	0.160	4.609(2)	55.84
tep02	0.02	—	0.092	5.493(2)	63.98
tep08	0.08	—	0.303	5.295(2)	66.93
tep14	0.16	0.14	0.449	4.958(2)	67.65
tep19	0.24	0.19	0.540	4.739(2)	68.68
tep27	0.32	0.27	0.649	4.339(2)	68.86
tep32	0.40	0.32	0.702	4.158(2)	69.62

incident energy spectrum which is needed for data normalization in the time-of-flight regime. The diffraction data were corrected using standard procedures for container and background scattering, attenuation, multiple scattering and inelasticity effects [24]. Finally, the differential scattering cross-sections, $d\sigma/d\Omega$, collected in the detector groups 2, 3, 4, and 5 are used. The corresponding functions of sample tep14 are shown in figure 1. An unusual feature exists in the data for $Q > 80$, 150, 270, and 400 nm^{-1}, respectively (Q is the momentum transfer with $Q = 4\pi/\lambda \cdot \sin\theta$, λ—radiation wavelength, 2θ—scattering angle). The strong decay is due to resonance effects of Te nuclei for epithermal neutrons of 2.3 eV. Another spurious but small decay visible in the data range 200 nm^{-1} $< Q <$ 400 nm^{-1} of detector group 5 was removed by an empirical function. For composing the final Faber–Ziman structure factors $S_N(Q)$ [25] the data of groups 2, 3 and 4 were adjusted to those of group 5.

The x-ray diffraction experiments were performed at the BW5 wiggler beamline at DORIS III of Deutsches Elektronen-Synchrotron (Hamburg). An incident photon energy of 122.7 keV ($\lambda = 0.0101$ nm) was chosen for the experiments. The beam size was 1×4 mm^2. Exact absorption corrections are difficult because the diameter of 1.5 mm of the silica capillaries (with wall thickness of 0.01 mm) containing the glassy powder exceeds the beam width.

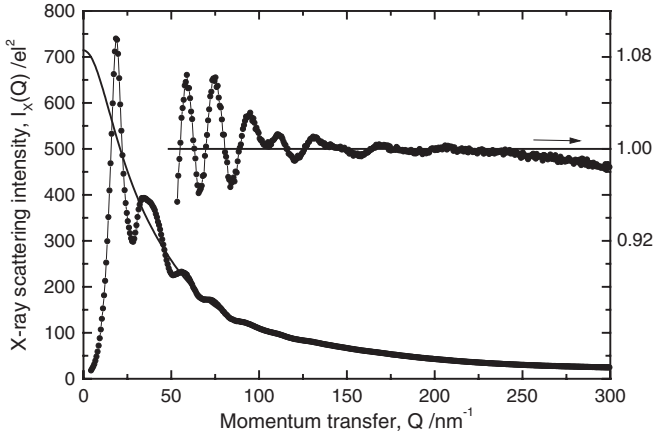

Figure 2. X-ray scattering intensities of sample tep14 after finishing all corrections and normalization. The solid-line function is the structure-independent scattering which is the sum of the compositional average of squares of atomic scattering amplitudes $\langle f^2(Q)\rangle$ and of the Compton scattering. The quotient of both functions is shown in the upper right section to visualize small normalization deficits in the high-Q range.

The scattering angles are small ($2\theta = 28°$ for $Q_{\max} = 300$ nm^{-1}) and the transmission coefficients are greater than 0.9 so that absorption is independent of the angle θ. The electronic energy window of the solid-state Ge detector was chosen to pass the elastic line and the full Compton peak but no fluorescence radiation. Dead-time corrections were made with parameter $\tau = 1.08\ \mu$s [26] and a fraction of 0.91 of incident photons is polarized horizontally. Corrections were made for background, container scattering, polarization and absorption. Subsequently, scattering intensities were normalized to the structure-independent scattering functions which were obtained from the tabulated atomic elastic scattering factors [27] and atomic Compton scattering data [28]. Figure 2 shows the scattering intensities of sample tep14 after normalization to the corresponding structure-independent scattering. A quotient of both functions is shown in the upper right section of the figure. The quality of data is satisfactory to obtain an excellent normalization. An empirical correction with a smooth function was used in the range of $Q >\sim 220$ nm^{-1} that makes the scattering intensity oscillate around the structure-independent scattering. Deficits in the calculation of the Compton fraction, uncertainties of the chemical compositions, errors in the instrument calibration and instabilities of beam position and of monitor efficiencies can cause the deviations. Finally, the Faber–Ziman structure factors, $S_X(Q)$, are calculated [25, 29].

3. Results

3.1. Structure factors and correlation functions

The neutron and x-ray structure factors shown in figures 3(a), (b) are weighted with Q to make visible the oscillations in the high-Q range. If compared with the other series only small changes of the corresponding functions are visible for the samples tek08, tek12 and tek16. But the K_2O contents of the K_2O–TeO_2 glasses are small if compared with the P_2O_5 contents of the other samples. For comparison of the structural effects of second oxides it is better to consider the fractions $c(M_zO)$ with M = K or P as given in table 1. Specific features of the structure factors of the K_2O–TeO_2 glasses are a double first peak in the $S_N(Q)$ data and a prepeak in

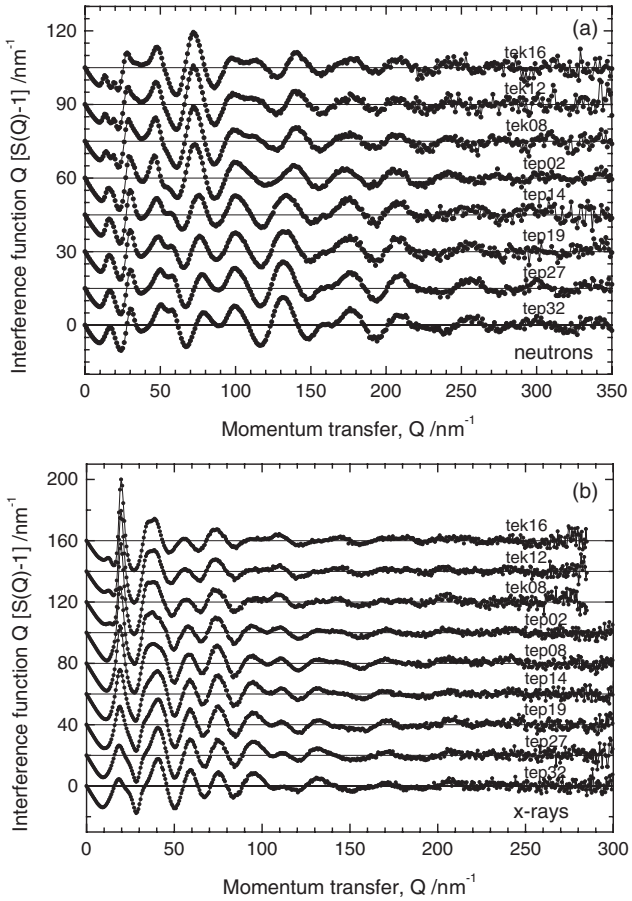

Figure 3. Weighted structure factors of the samples studied: (a) neutron data and (b) x-ray data. Upper functions are shifted for clearness of the plot.

the $S_X(Q)$ data whose height increases with increasing K_2O content. Such features were also found by other authors [16–18]. On the other hand, strong systematic changes accompanying the growing P_2O_5 content exist in the structure factors of the P_2O_5–TeO_2 series. The diffraction data of sample tep02 are similar to those reported by Neov *et al* [23]. Different from most earlier work [16–18] greater Q-ranges were realized in our experiments. The better resolving power and the combination of neutron and x-ray data help to extract more details of the Te–O first-neighbour peaks, and thus about the TeO_n structural units. The data of high Q-values are important to resolve detailed information of the narrow peak components of the covalent bonds. The truncation effects of Q_{max} in the Fourier transformations (FT) are reduced evidently with Q_{max} of 400 or 280 nm^{-1} for the neutron or x-ray data. The real-space correlation functions, $T(r)$, are calculated with

$$T(r) = 4\pi r\rho_0 + 2/\pi \int_0^{Q_{max}} Q[S(Q) - 1]M(Q)\sin(Qr)\,dQ. \quad (1)$$

Here ρ_0 is the number density of atoms (table 1). The function $M(Q)$ is introduced to damp spurious features such as ripples caused by noise and by termination of the Fourier integral at Q_{max}. The function $M(Q)$ used is $M(Q) = \sin(\pi Q/Q_{max})/(\pi Q/Q_{max})$ [30]. The resulting

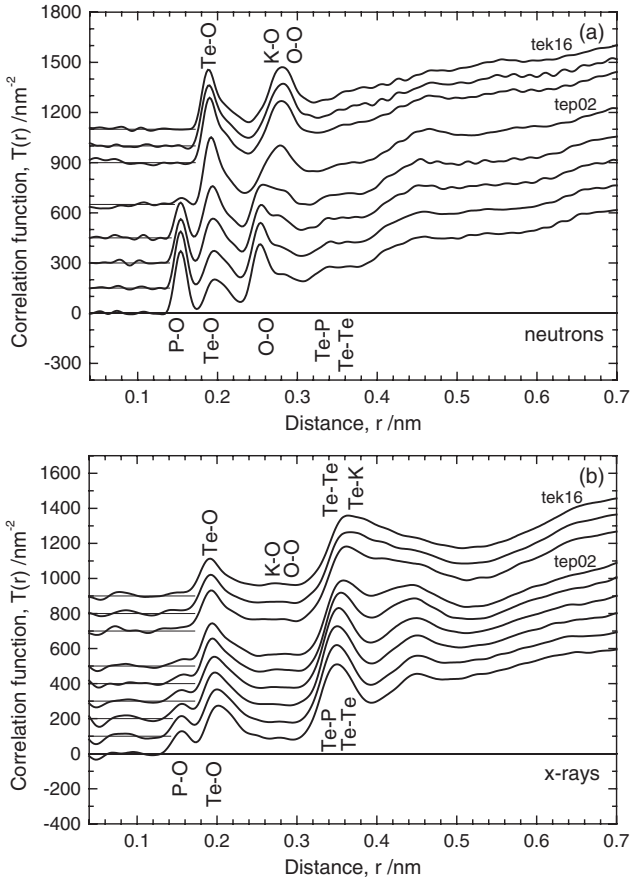

Figure 4. Correlation functions of all samples obtained with Fourier transformation using damping and $Q_{\max}$ of 400 nm^{-1} for the neutron data (a) and 280 nm^{-1} for the x-ray data (b). The $T(r)$ functions of the different samples are plotted in the same order as in figure 3. Upper functions are shifted for clearness of the plot.

$T(r)$ functions are compared in figure 4. The peak broadening is already a small effect with $Q_{\max}$ of 400 nm^{-1}. Thus, the neutron $T_N(r)$ functions show nearly all details of peaks of the glass structure which could be extracted. The P–O peaks are narrower in the $T_N(r)$ functions obtained without damping but the corresponding satellite oscillations make peak fits more difficult. Hence, $T(r)$ functions obtained with damping as shown in figure 4 are used in the peak fitting. A good agreement between the $T(r)$ functions obtained without damping and the corresponding model $T(r)$ functions calculated with the final peak parameters was achieved in most cases, as well. But a few of the $T(r)$ functions obtained without damping show some unphysical features and, therefore, they are not used and not shown.

3.2. Gaussian fitting of the first-neighbour peaks

The height of the P–O peak of bond lengths of ∼0.155 nm grows continuously with the P_2O_5 content. The fit of this peak is made by a single Gaussian function. A sharp Te–O peak follows at ∼0.19 nm which is accompanied by a long tail extending to 0.24 nm (cf figure 4). Other distances are not expected in this range. Thus, clear information is obtained for the

Table 2. Parameters resulting from Gaussian fitting of the Te–O, K–O and O–O first-neighbour peaks of the K_2O–TeO_2 glasses. Numbers in parenthesis give the uncertainty in the last digit. The parameters of the K–O peak are fixed identical for all three samples of this series as given for tek08. The total Te–O coordination numbers take into account only the bonds with lengths less than 0.23 nm. N_{short} and N_{long} contain bond lengths of 0.19 and 0.20–0.23 nm, respectively.

Sample	Atom pair	Peak parameters			Total coordination number	N_{short}	N_{long}
		N_{ij}	r_{ij} (nm)	Δr_{ij} (nm)			
tek08	Te–O	1.90	0.189(1)	0.013(2)	3.90(10)	1.90(10)	2.00(20)
		1.05	0.203[a]	0.018(3)			
		0.95	0.220[a]	0.027(4)			
		0.60	0.255[a]	0.028[a]			
		0.40	0.280[a]	0.030[a]			
	K–O	3.00[a]	0.267[a]	0.015[a]			
		4.00[a]	0.288[a]	0.035[a]			
	O–O	5.04	0.282	0.036			
tek12	Te–O	1.95	0.188(1)	0.015(2)	3.85(10)	1.95(10)	1.90(20)
		0.95	0.203[a]	0.017(3)			
		0.95	0.220[a]	0.027(4)			
		0.50	0.255[a]	0.028[a]			
		0.30	0.280[a]	0.030[a]			
	O–O	5.10	0.284	0.036			
tek16	Te–O	1.90	0.189(1)	0.014(2)	3.75(10)	1.85(10)	1.90(20)
		0.85	0.203[a]	0.018(3)			
		1.00	0.220[a]	0.032(4)			
		0.40	0.255[a]	0.028[a]			
		0.33	0.280[a]	0.030[a]			
	O–O	4.46	0.284	0.034			

[a] These values are fixed in the fits.

Te–O bond lengths. From knowledge of the structure of the related crystals $P_2Te_4O_{13}$ [31] and $P_2Te_3O_{11}$ [32] we can assume that except for the short P–O bonds other than Te–O and O–O distances do not exist for lengths less than ∼0.29 nm (cf section 4.3). An unequivocal fit of Te–O and O–O distances is possible in this r-range because two data sets, the $T_N(r)$ and $T_X(r)$ functions, are available. For the K_2O–TeO_2 glasses, additionally, a broad peak of K–O distances is expected at ∼0.275 nm which superposes with the lengths of the O–O edges of the TeO_n groups and possible longer Te–O distances. However, the contribution of K–O distances is small in both $T(r)$ functions. Fits with fixed parameters of the K–O first-neighbour peaks are justified. Approximate parameters taken from earlier diffraction work (KPO_3 glass [33]) and from structures of K tellurite crystals [34] are used for the K–O peak. The fixed parameters are given below in table 2.

As already realized in our earlier diffraction work of tellurite glasses [35, 36] the Te–O first-neighbour peak is fitted with three Gaussian functions. A few possible longer Te–O distances are approximated with broad Gaussian functions with fixed distances of 0.240 (0.255) and 0.280 nm. The O–O peak of K_2O–TeO_2 glasses is approximated with a single Gaussian function at ∼0.28 nm. This approach was successful in the analysis of the V, Zn and Nb tellurite glasses studied earlier [35, 36]. In the case of the P_2O_5–TeO_2 glasses, additionally, a sharp peak of O–O distances occurs at ∼0.252 nm (cf figure 4(a)) which belongs to the edges of the PO_4 tetrahedra. Thus, two or three Gaussian functions are used for the O–O contribution in the case of the P_2O_5–TeO_2 glasses. The broad Gaussian functions used form

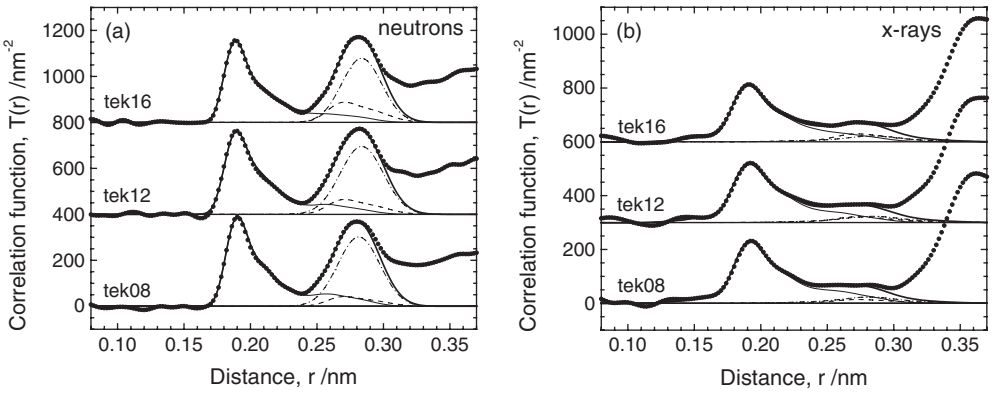

Figure 5. Correlation functions in the range of the first-neighbour peaks of the K_2O–TeO_2 glasses (dotted lines): (a) neutron and (b) x-ray data. The model $T(r)$ functions are given as thick solid lines; the partial correlations are given as thin solid lines (Te–O), dashed lines (K–O) and dash–dotted lines (O–O).

rather continuous Te–O, O–O and K–O distance distributions. The analysis of distributions is stopped at ∼0.29 nm. Most of the Gaussian functions do not form well resolved peaks and, thus, should not be interpreted to represent specific types of bonds. An exception was the differentiation made in [35, 36] for short and long Te–O bonds of ∼0.19 and ∼0.21 nm of the TeO_n structural groups. The fractions of these bonds confirm the existence of TeO_4 and TeO_3 units as trigonal bipyramids (tbps) and trigonal pyramids (tps). Here and below notations concerning the Te–O coordination state are used in the classical sense, i.e. regarding only bond lengths less than 0.23 nm. A similar character of the Te–O peak is visible for the K_2O–TeO_2 glasses and for sample tep02 (cf figure 4). The dominance of a narrow component at ∼0.19 nm is lost for the Te–O peaks of the other P_2O_5–TeO_2 glasses due to increasing fractions of distances greater than 0.20 nm.

Gaussian fitting is performed to the $T_N(r)$ and $T_X(r)$ data simultaneously. The model $T(r)$ functions fit the experimental data up to lengths of 0.28 nm. The effects caused by termination of FT at $Q_{\max}$ are taken into account by convolution of the model Gaussian functions with peak functions, $P_{ij}(r)$, which simulate the Q-window and damping used in equation (1) [37, 38]. The parameters are the coordination numbers, N_{ij}, the mean distances, r_{ij}, and the peak widths (full widths at half maximum), Δr_{ij}, for pairs of atomic species i and j. Least-squares fits are performed using the Marquardt algorithm [39]. The constraints and parameters fixed in the fits have been varied several times to find the optimum set of Gaussian functions that is needed to approximate the experimental $T(r)$ functions. Starting parameters for the Te–O peak are chosen as reported before [35, 36].

3.3. Fit results of the K_2O–TeO_2 glasses

The successful fits of the $T(r)$ functions of the K_2O–TeO_2 glasses are shown in figure 5 and the corresponding parameters of the Gaussian functions are given in table 2. The resulting parameters show that with decreasing K_2O content and approaching pure TeO_2 glass N_{TeO} approaches four, which indicates the existence of TeO_4 units. TeO_3 units are formed with increasing K_2O content. But the clear separation into a narrow and a broad peak component as was successful in the earlier work [35, 36] is not well developed. If the Te–O peak is assumed to be formed of two components, the first with distances of 0.19 nm and the second with

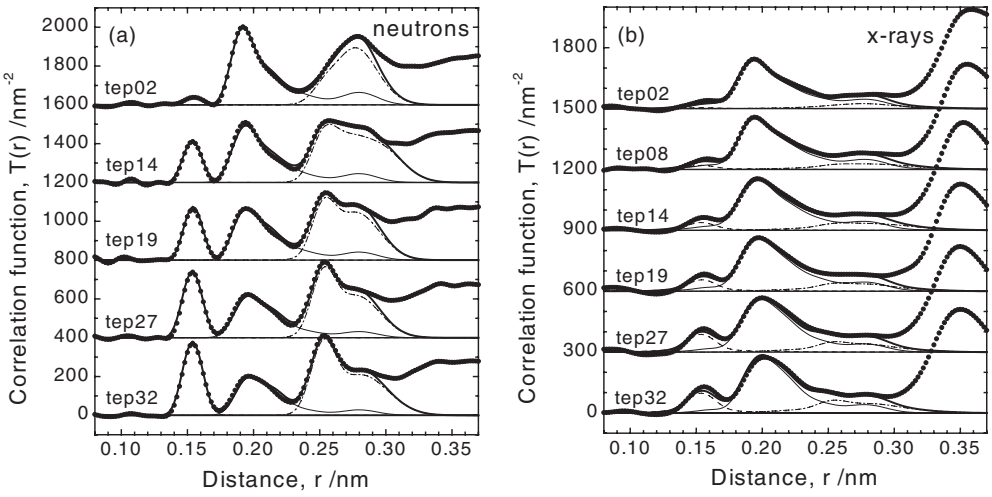

Figure 6. Correlation functions in the range of the first-neighbour peaks of the P_2O_5–TeO_2 glasses (dotted lines): (a) neutron and (b) x-ray data. The model $T(r)$ functions are given as thick solid lines; the partial correlations are given as dashed lines (P–O), thin solid lines (Te–O) and dash–dotted lines (O–O).

distances ranging from 0.20 to 0.22 nm, equal fractions of short Te–O_{eq} and longer Te–O_{ax} bonds are found which is typical for TeO_4 tbp units (cf table 2, illustrations of the units in section 4.2). The increase of the fraction of short Te–O bonds expected as an accompanying effect of the increase of the number of TeO_3 at the expense of TeO_4 units reported for glasses of higher modifier content [35, 36] is not significant for our short series of K_2O–TeO_2 glasses.

Supposing the uncertainty of the assumptions made for the model K–O distance peak is small, so the fit yields clear indications for the existence of Te–O distances beyond typical bond lengths (>0.23 nm). Te–O distances of 0.255 nm have to be taken into account which is especially needed to fit the x-ray results (figure 5(b)). Such distances can belong to TeO_{3+1} units as the additional longer bond. But also the Te atoms in TeO_4 units can possess additional oxygen neighbours, for example, forming distorted TeO_6 octahedra as are known of the TeO_2 polymorphs [40–42] (cf section 4.2). A next small contribution is assumed at 0.280 nm but here the separation of different partials becomes already questionable. The sums of bond valencies, S_{bv}, of the TeO_n units [43] with i running from 1 to 5 with the ith Te–O distances r_i and weights N_i (table 2) are checked with

$$S_{bv} = \Sigma_i N_i 1.333\ (r_i/0.1854)^{-5.2}. \tag{2}$$

The S_{bv} result in 3.8–3.9 (four is expected for Te(IV) atoms) which confirms the fit approach used. The total number of oxygen neighbours up to distances of 0.28 nm obtained in the fits decreases from 4.9 for sample tek08 to 4.6 for sample tek16.

3.4. Fit results of the P_2O_5–TeO_2 glasses

The fit results of the P_2O_5–TeO_2 glasses are shown in figure 6 and the corresponding parameters of the Gaussian functions are given in table 3. A first analysis of the $T(r)$ functions using the nominal compositions (table 1) has led to unexpected small P–O coordination numbers, N_{PO}, of 3.5–3.6 accompanied by high N_{TeO} numbers up to ∼6. Loss of volatile P_2O_5 could explain this behaviour. Therefore, the P_2O_5 contents are varied for samples tep14, tep19, tep27, and

Table 3. Parameters resulting from Gaussian fitting of the Te–O, P–O, and O–O first-neighbour peaks of the P_2O_5–TeO_2 glasses. The numbers in parenthesis give the uncertainty in the last digit.

	Te–O coordination			Atom	P–O and O–O coordination		
Sample	N_{TeO}	r_{TeO} (nm)	Δr_{TeO} (nm)	pair	N_{ij}	r_{ij} (nm)	Δr_{ij} (nm)
tep02	1.90	0.190(1)	0.014(2)	P–O	4.00[a]	0.155(1)	0.007(5)
	1.35	0.206	0.024				
	0.75	0.220[a]	0.035	O–O	0.45	0.252[a]	0.017
	0.35	0.240[a]	0.030[a]		2.39	0.275	0.032
	0.95	0.280[a]	0.030[a]		2.53	0.280	0.040[a]
tep08	1.85	0.190(1)	0.014(2)	P–O	4.00[a]	0.154(1)	0.011(3)
	1.40	0.206	0.022				
	0.90	0.220[a]	0.030	O–O	0.80	0.252[a]	0.015
	0.40	0.240[a]	0.030[a]		2.20	0.266	0.030
	1.00	0.280[a]	0.030[a]		3.40	0.293	0.040[a]
tep14	1.90	0.191(1)	0.017(2)	P–O	4.00[a]	0.154(1)	0.011(2)
	1.33	0.206	0.025				
	0.95	0.218[a]	0.029	O–O	1.70	0.252[a]	0.019
	0.48	0.240[a]	0.030[a]		1.86	0.269	0.028
	0.87	0.280[a]	0.030[a]		3.54	0.294	0.040[a]
tep19	1.55	0.191(1)	0.014(2)	P–O	4.00[a]	0.154(1)	0.011(2)
	1.85	0.206	0.024				
	0.91	0.218[a]	0.033	O–O	1.72	0.252[a]	0.016
	0.55	0.240[a]	0.030[a]		4.26	0.278	0.040
	0.88	0.280[a]	0.030[a]				
tep27	2.10	0.190(1)	0.018(2)	P–O	4.00[a]	0.154(1)	0.013(2)
	1.66	0.212	0.022				
	0.70	0.220[a]	0.037	O–O	2.23	0.252[a]	0.017
	0.50	0.240[a]	0.030[a]		1.78	0.275	0.038
	0.80	0.280[a]	0.030[a]		1.91	0.280	0.040
tep32	2.00	0.190(1)	0.017(2)	P–O	4.00[a]	0.154(1)	0.013(2)
	1.80	0.212	0.021				
	0.80	0.220[a]	0.035	O–O	2.70	0.252[a]	0.019
	0.40	0.240[a]	0.030[a]		2.16	0.276	0.039
	0.80	0.280[a]	0.030[a]		1.78	0.291	0.042

[a] These values are fixed in the fits.

tep32 and the corresponding N_{PO} numbers are determined. Finally, those compositions are chosen for which N_{PO} equals four. The change of P_2O_5 content of sample tep02 is negligible. A neutron diffraction experiment was not successful for sample tep08 and, thus, an improvement of the corresponding glass composition is not possible. In addition to the three Gaussian functions used to approximate the Te–O bonds also two further peaks with Te–O distances of 0.240 and 0.280 nm are used. The sums S_{bv} calculated according to equation (2) give values very close to the expected number of four. This behaviour confirms the final P_2O_5 contents used in the data analyses. S_{bv} values of four are also obtained for the TeO_n units of the related crystal structures [31, 32]. The fits shown in figure 6 are not fully successful for distances ranging from 0.21 to 0.23 nm. The origin of these small differences between the neutron and x-ray $T(r)$ functions could not be clarified. The total number of oxygens bonded to the Te atoms is four for sample tep02 and it increases up to 4.6 for the sample of highest P_2O_5 content studied (32 mol%). If the more distant oxygen atoms up to 0.28 nm are also taken into account the total Te–O coordination numbers behave as constant at ∼5.7 which gives support to the

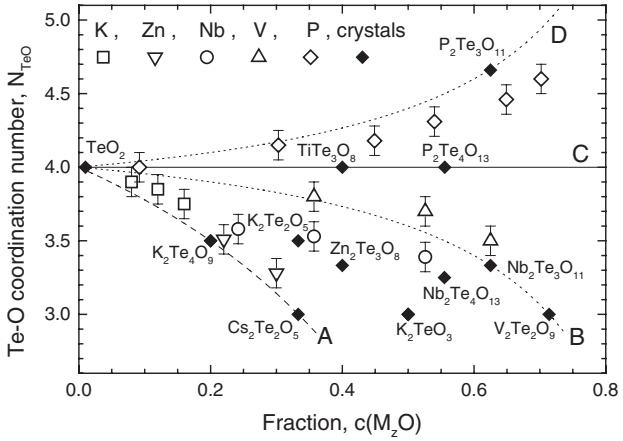

Figure 7. Behaviour of the Te–O coordination numbers of the K_2O–TeO_2 and P_2O_5–TeO_2 glasses studied and of N_{TeO} values reported for tellurite glasses with V_2O_5 [35], ZnO and Nb_2O_5 [36] additions. Note that only typical bond lengths less than 0.23 nm are taken into account for the N_{TeO} presented. The N_{TeO} numbers are compared with those of some related crystal structures (TeO_2 [40–42], $P_2Te_3O_{11}$ [31], $P_2Te_4O_{13}$ [32], $K_2Te_4O_9$ $K_2Te_2O_5$ [34], $TiTe_3O_8$ [50], $Cs_2Te_2O_5$ [51], K_2TeO_3 [52], $Zn_2Te_3O_8$ [53], $Nb_2Te_4O_{13}$ [54], $Nb_2Te_3O_{11}$ [55], $V_2Te_2O_9$ [56]). Details are discussed in sections 4.2 and 4.3. The dashed, dotted and solid lines specify behaviour of N_{TeO} according to four models of changes of TeO_n groups. The models are described in the text.

existence of distorted TeO_6 octahedra in the P_2O_5–TeO_2 glasses studied. The numbers of O atoms with typical bond lengths show an unusual increase. Please note that the sums S_{bv} of the Te(IV) atoms are constant at four and independent of the P_2O_5 content. Increasing Te–O bond lengths compensate for the increase of N_{TeO}.

The lengths of the P–O bonds at 0.154 nm match those found for other phosphate glasses [44]. Widths Δr_{PO} of this peak at ∼0.012 nm are typical values for single types of bonds, either P–O_B or P–O_T (O_B bridging, O_T terminal oxygen). Hence it follows that preferably isolated PO_4 tetrahedra (no P–O–P bridges but only P–O–Te links) with four equivalent P–O_T bonds (bond valency of ∼1.25) are spread in the tellurite network. Such behaviour of PO_4 units is known for phosphate glasses of small P_2O_5 content [45, 46]. The component at 0.252 nm in the O–O correlations increasing with the P_2O_5 content is caused by the edges of the PO_4 tetrahedra. A precise determination of the number of edges is not possible due to the overlap with O–O edge lengths of the TeO_n polyhedra.

4. Discussion

4.1. Changes of the TeO_n groups in dependence on different second oxides

The Te–O coordination numbers obtained in the diffraction experiments are plotted in figure 7 where also earlier results of V, Zn and Nb tellurite glasses are shown [35, 36]. Also other authors [23, 47–49] reported Te–O coordination numbers of modified tellurite glasses obtained in diffraction experiments of high resolving power. Numbers N_{TeO} are similar to our results. However, these N_{TeO} are not shown in figure 7 because we do not want to mix results analysed in different ways. Please note that only Te–O bonds of lengths less than 0.23 nm are taken into account for the N_{TeO} shown. Four of the samples studied possess only small fractions $c(M_zO)$ of second oxide. The corresponding N_{TeO} numbers tend to four in the compositional limit of a

glass of pure TeO_2. In the opposite direction, with increasing $c(M_zO)$ fractions, the behaviour of N_{TeO} strongly depends on the atomic species M.

Figure 7 shows also the N_{TeO} of related crystal structures. Analysis of the TeO_n units of these structures already reveals the problem: for presentation of the N_{TeO} of the crystals all TeO_n polyhedra have been classified into units with $n = 3$, 4 and 5 taking into account only distances shorter than 0.23 nm. According to [12, 57] these Te–O distances belong to 'strong' bonds. Some units possess longer Te–O distances up to 0.26 nm ('medium' bond strength) which are called TeO_{n+m} units where m indicates the number of 'medium' bonds. Finally, most Te-centred oxygen polyhedra are completed by O atoms in 'weak' bonds situated next to the LPE of the Te(IV) atom. These bonds possess greater lengths in an interval from 0.26 to 0.32 nm. For these distances a clear differentiation from Te–O second neighbours is already difficult.

Analysis of our diffraction data of glasses results in continuous $T_{TeO}(r)$ functions where five Gaussian functions have been used to approximate their shape. For the K_2O–TeO_2 samples we have to assume a mixture of TeO_4 and TeO_3 units where, probably, the TeO_3 can be called TeO_{3+1} units due to Te–O 'medium' bonds approximated with the Gaussian peak at 0.255 nm. But some of these distances can also belong to TeO_4 units and further differentiation of types of polyhedra is not possible from diffraction results. The total number of O neighbours including those of the Gaussian function at 0.28 nm is less than five and it decreases with increasing K_2O content.

The N_{TeO} numbers of the P_2O_5–TeO_2 glasses increase to values greater than four with increasing P_2O_5 content. Mixtures of TeO_4 and TeO_5 units have to be assumed. The fraction of Te–O bond lengths ranging from 0.20 to 0.22 nm exceeds that of lengths of ∼0.19 nm. Clear differentiation into fractions N_{short} and N_{long} as made for the K_2O–TeO_2 glasses is not possible. Details of the conformations of TeO_4 and TeO_5 groups cannot be extracted. If the complete first-neighbour environments with distances up to 0.28 nm are taken into account, distorted TeO_6 octahedra exist for all glasses of different P_2O_5 content. The existence of Te–O first-neighbour distances ranging from 0.23 to 0.32 nm is also a fact for TeO_n groups in the glasses. Before more of the corresponding details of the glasses studied are discussed and compared with those of the related crystal structures (next sections) the general behaviour of the structural groups is considered.

For a general view it is useful to restrict the discussion to those N_{TeO} values which are determined as 'strong' bonds with lengths less than 0.23 nm. The numbers N_{TeO} can be related directly to the fractions of the different units. Therefore, it is sufficient to discuss the behaviour of N_{TeO}. Figure 7 shows the great variability of TeO_2 forming structural units which also reveals its intermediate character forming binary glasses. The oxygen added does not simply disrupt network bridges. In dependence on the coordination preferences of the atomic species M of the second oxide M_zO the number of terminal oxygens (O_T) can be increased by changing some TeO_4 having one O_T to TeO_3 units having two O_T where the electron charge and new Te=O double bond are delocalized on both Te–O_T bonds. The behaviour of N_{TeO} shown with the dashed-line function in figure 7 would be valid if a maximum of $TeO_4 \rightarrow TeO_3$ transitions were realized (model A) where N_{TeO} is calculated with

$$N_{TeO} = 4 - 2\,c(M_zO)/c(TeO_2). \tag{3}$$

From spectroscopic data of tellurite glasses modified with Li_2O, Na_2O, BaO and ZnO [58] this behaviour was suggested to be valid in the limit of small modifier additions. ^{125}Te nuclear magnetic resonance (NMR) spectroscopy has shown similar behaviour for tellurite glasses with M = La, Na, K, Rb, Cs [22], M = Mg, Zn, Sr, Ba, Pb [59] and M = Al, Ga [60]. Our diffraction results confirm this behaviour for tellurite glasses with ZnO [36] and K_2O (this work). Actually,

the real N_{TeO} numbers are little greater than predicted by model A which means that also TeO_4 with O_T still exist. This fraction increases with further modifier additions [22, 58–60]. Four O_T are formed for every oxygen added if model A is valid. Consequently, for M = Al and Ga a behaviour according to model A is only advantageous if the M–O coordination numbers are equal to six. In the process of increasing contents of M = Al, Ga mixed coordination states of the M sites were found (AlO_4, AlO_5, AlO_6 units [60]; GaO_4, GaO_6 units [60, 61]) where MO_n groups of greater n dominate for glasses of small M_zO content. Reduced effects of $TeO_4 \rightarrow TeO_3$ transition should occur for oxides M_zO of even smaller z and/or N_{MO} (with $z < 2/3$ and $N_{MO} < 6$).

For tellurite glasses with M = Nb [36] or V [35] the $TeO_4 \rightarrow TeO_3$ transition is strongly reduced. An increasing fraction of TeO_4 units with O_T exists. The N_{TeO} numbers shown for V_2O_5–TeO_2 glasses [35] are close to a model B which was suggested [62] according to ^{125}Te NMR results (dotted line dropping down). Only 20% of the oxygens added act in the sense of model A. V–O–V (or Nb–O–Nb) bridges occur for greater fractions of second oxide [35, 36, 62] which indicate for the second component likewise network-forming character. For these glasses the definitions of O_B and O_T atoms become problematic due to coexistence of two network-forming oxides. Decreasing values of N_{MO} numbers with transitions from VO_5 to VO_4 units [35, 62] and from NbO_7 to NbO_6 polyhedra [36] are found with increasing M_zO content.

Though binary tellurite glasses are also formed with many of the typical glass-forming oxides [63] (not with SiO_2), structural investigations of such series are rare. Note that in this kind of binary systems stable and metastable immiscibility could occur [64]. Obviously, also for the B_2O_3–TeO_2 or GeO_2–TeO_2 glasses the higher M–O coordination states are realized, thus, with BO_4 tetrahedra (^{11}B NMR [65]) or large fractions of GeO_6 octahedra (Ge K-edge EXAFS [66]). The fraction of GeO_6 octahedra decreases with increasing GeO_2 content [66]. It seems that TeO_4 tbps dominate the tellurite networks of both glass series independent of the M_zO content [13, 67]. Model C characterizes this behaviour (solid line in figure 7). If only TeO_4 units coexist with the BO_4 or GeO_6 groups some oxygens of the MO_n groups have to be linked with two Te.

Finally, the effect of P_2O_5 is discussed. The analysis is started from the point of view of binary phosphate glasses. Different from B or Ge the P atoms do not increase the number of their oxygen neighbours. Since phosphorus has valency five but forms PO_4 tetrahedra one of the oxygens has to form a double bond as found in vitreous P_2O_5 [68, 69]. All O atoms of other oxides added are used to disrupt P–O–P bridges [70], and all oxygens of P–O bonds outside these bridges tend to coordinate groups of the second component [71]. π-bonding in the PO_4 units is delocalized on more and more P–O bonds not being members of P–O–P bridges [72]. Isolated PO_4 units are formed in the limit of full degradation of the phosphate networks [45, 46] with four equivalent P–O bonds of bond valency ∼1.25. This compositional point is reached at molar ratio $y = c(Te_{0.5}O)/c(P_2O_5)$ equal to 3 [70]. In the notation of compositions used above this means tellurite glasses with 40 mol% P_2O_5 or $c(M_zO) = \sim 0.77$. The critical number, M_{TO}, of oxygens available for coordination of each Te is $M_{TO} = v(y + 1)/y$ (v—valency of Te) [71]. M_{TO} is equal to ∼5.3 for $y = 3$. Now the calculation of M_{TO} is extended to glasses of smaller P_2O_5 content and M_{TO} is written in the notation used in equation (3). The Te–O coordination number is equal to M_{TO} if every O atom is either in a P–O–Te or in a Te–O–Te bridge. In this case N_{TeO} varies with the composition by

$$N_{TeO} = 4 + 0.4\, c(P_{0.4}O)/c(TeO_2). \tag{4}$$

The corresponding behaviour of TeO_n units is called model D. The change of N_{TeO} is shown in figure 7 with the dotted line rising. This behaviour translated into fractions of groups means

one TeO_4 is changed to a TeO_5 unit for every PO_4 unit added. For a greater P_2O_5 content TeO_6 units should also exist. The experimental N_{TeO} show a trend according to model D but with values being little smaller than those expected (figure 7). The remaining differences can have several reasons: the P_2O_5 contents of the glasses studied possess some uncertainty (cf sections 2 and 3.4). Moreover, TeO_n units are highly asymmetric due to LPE effects. Additional oxygens may persist in 'medium' Te–O bonds with lengths greater than 0.23 nm which are not included in the N_{TeO} values shown in figure 7.

Above it was assumed that all O atoms form either P–O–Te or Te–O–Te bridges. If in fact some O atoms were to coordinate more than two Te (or P) the N_{TeO} values should increase more than predicted. This situation could exist if all O neighbours found in 'medium' and 'weak' Te–O bonds with lengths up to 0.28 nm were included in the considerations. In contrast, effects which could maintain smaller N_{TeO} values close to four would be the formation of localized double P=O or Te=O bonds with oxygens not coordinating second neighbours. The corresponding bond lengths should be clearly shorter than those observed. Significant fractions of such bonds are not detected. The increase of N_{TeO} for P_2O_5–TeO_2 glasses results from the strong effect of PO_4 units forcing the Te(IV) to accept an increased number of O neighbours. In this process the sums S_{bv} of Te(IV) according to equation (2) [43] are constant where the increase of N_{TeO} is compensated by an elongation of the Te–O bonds.

4.2. Structural groups of related crystal structures

The diffraction results contain more information than only Te–O coordination numbers. The $T(r)$ functions reveal details of the Te–O and O–O correlations up to distances of 0.28 nm. Comparisons with the partial correlation functions calculated for related crystal structures should allow us to extract more features of the glass structures. The geometries of some polyhedra of relevant crystal structures are presented before the comparisons are started. The structural units are named TeO_{n+m} which means they have n 'strong' and m 'medium' Te–O bonds. Since the tek08 and tep02 samples have compositions close to that of vitreous (v-)TeO_2 the corresponding TeO_4 tbps of the three known TeO_2 polymorphs [40–42] are also shown (upper part of figure 8). Strictly speaking, the TeO_4 unit is a disphenoid [42]. Only if the corner with the LPE is taken into account can a distorted trigonal bipyramid be imagined. As well as the four oxygens in 'strong' bonds (circles with hatched filling) two 'weakly' bonded oxygens (open circles) also exist. The centre of negative charge of the LPE is located close to the Te site in the triangle formed of Te and the two 'weakly' bonded O. The TeO_4 tbps of α-TeO_2 [40] possess a high symmetry which is lost for the TeO_4 of β- [41] and γ-TeO_2 [42]. The distortions result in unlike lengths of both Te–O_{ax} bonds. The shifts seem to be changes toward the geometry of the TeO_{3+1} unit which is shown for $K_2Te_4O_9$ [34]. The TeO_{3+1} unit possesses an O atom (circle filled with dots) of 'medium' bond strength. The TeO_{3+1} units themselves are understood as transitional groups in the change to real TeO_3 tps like that shown for $K_2Te_2O_5$ [34]. With P_2O_5 additions, the numbers of O atoms in 'strong' and 'medium' Te–O bonds increase in steps of the TeO_{4+1} and TeO_5 units.

The 'strong' bonds of TeO_4 tbps are differentiated into two short Te–O_{eq} and two long Te–O_{ax} ($\sim$0.19 and $\sim$0.21 nm) while TeO_3 units have only short 'strong' bonds (figure 8). This differentiation was successful for the Te–O peaks of tellurite glasses from earlier diffraction experiments using also high resolving power [35, 36]. Fractions of TeO_4 and TeO_3 units could be analysed considering the fractions of short and longer bonds, where possible TeO_{3+1} were related to the TeO_3 fraction. The same detailed fit was made for the Te–O peaks of the $T(r)$ data in the present study. A similar differentiation of lengths was successful for the tek08, tek12, tek16 and tep02 samples. The procedure results in equal fractions of short

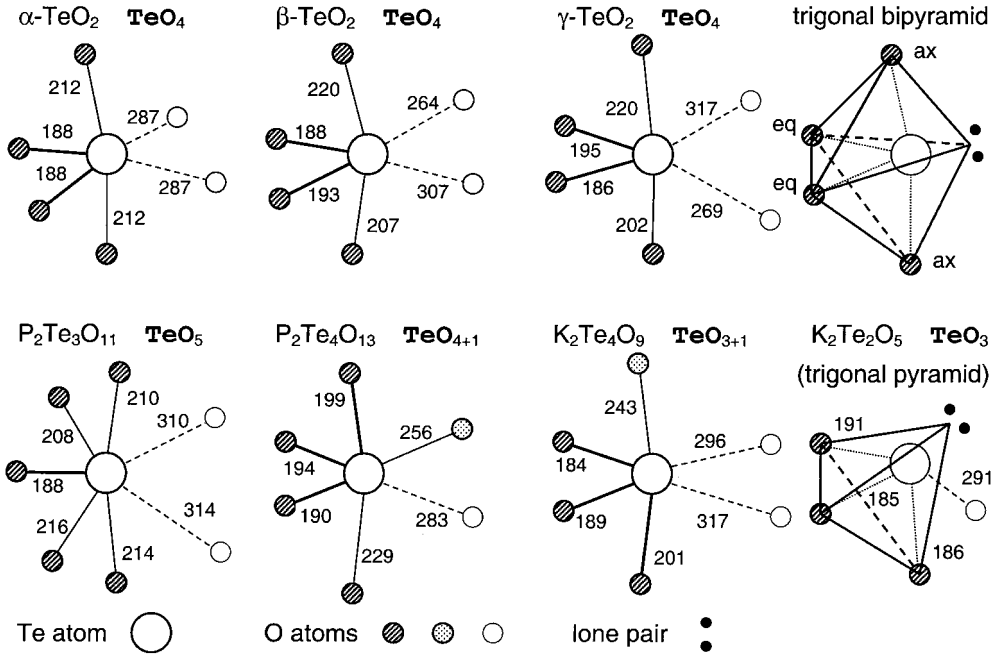

Figure 8. TeO_n polyhedra of related tellurite crystals. Upper part: TeO_4 trigonal bipyramids (tbps) known of α-TeO_2 [40], β-TeO_2 [41] and γ-TeO_2 [42]. Lower part: TeO_{3+1} units in $K_2Te_4O_9$ [34] and TeO_3 trigonal pyramids (tps) in $K_2Te_2O_5$ [34], as well as TeO_5 units in $P_2Te_3O_{11}$ [31] and TeO_{4+1} units in $P_2Te_4O_{13}$ [32]. Circle filling denotes O atoms in 'strong' (hatched), 'medium' (dotted) and 'weak' (no filling) Te–O bonds with distances $r_{TeO} < 0.23$ nm, $0.23\ \text{nm} < r_{TeO} < 0.26$ nm and $0.26\ \text{nm} < r_{TeO} < 0.32$ nm where the thick solid lines accentuate the shortest 'strong' bonds. Bond lengths are given in picometres.

and long bonds (tables 2, 3). But the increase of the fraction of shorter bonds as expected for an increasing number of TeO_3 units with increasing K_2O content in K_2O–TeO_2 glasses is not found. This poor resolution can be due to the great fraction of TeO_{3+1} which show more varieties of conformations than the TeO_3 tps. Also the TeO_4 units might have stronger distortions with the higher network connectivity in glasses of little modifier content. The results reported before [35, 36] were obtained for glasses of higher modifier content $c(M_zO)$.

The Te–O bonds in the TeO_5 and TeO_{4+1} units of the $P_2Te_3O_{11}$ [31] and $P_2Te_4O_{13}$ [32] crystals do not allow us to classify the units into types with definite numbers of short and long bonds. Units of other distortions than those shown in figure 8 also exist in these crystals. Thus, already the TeO_n units of the crystals show that model D can give only an approximate description of N_{TeO} behaviour due to geometrical variations with an intermixing of short and long 'strong', 'medium' and 'weak' Te–O bonds. The shapes of the Te–O peaks indicate a non-continuous behaviour. The Te–O peaks of the glasses tep02, tep08, tep14 and tep19 (figures 4, 6) show the typical narrow component at ∼0.19 nm accompanied by a flat tail on the side of longer distances where the Te–O peak of tep19 is already broader. Different from that the Te–O peaks of samples tep27 and tep32 show two clear components at ∼0.195 and ∼0.210 nm. A possible explanation of this change is connected with a next deficit of model D: it was assumed that only TeO_4 and TeO_5 units coexist. The latter are needed to compensate for the PO_4 tetrahedra. But flexible TeO_n units can form intermediate structures such as TeO_{4+1}. All TeO_n surrounding a PO_4 tetrahedron participate in its charge compensation. For

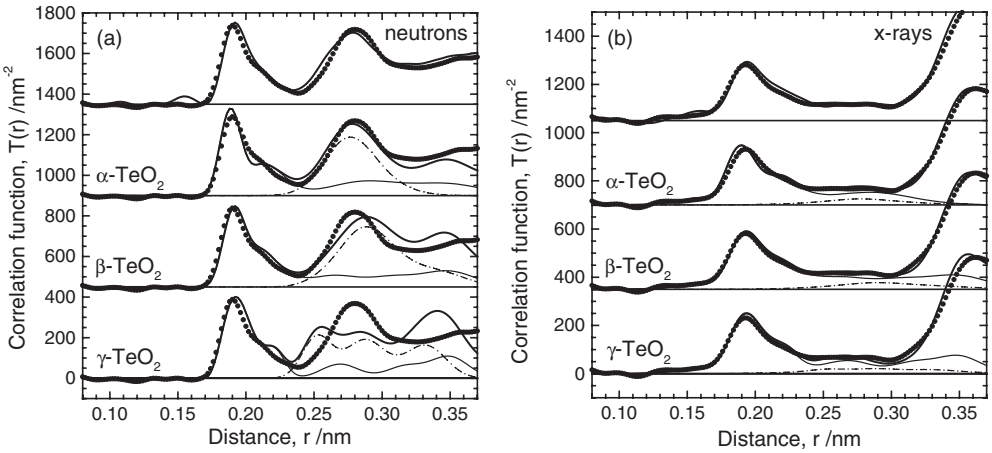

Figure 9. The experimental $T(r)$ functions (dots) of sample tek08 obtained from neutron (a) and x-ray (b) data compared with model $T(r)$ functions (thick solid lines) calculated by use of the SRO of polymorphs α- [40], β- [41] and γ-TeO_2 [42]. Partial correlations: Te–O—thin solid lines; O–O—dash–dotted lines. On top, the $T(r)$ functions of tek08 are compared with those of tep02 sample (solid lines).

small P_2O_5 content the compensation is preferably realized with TeO_{4+1} units. For glasses of $c(M_zO)$ content of $\sim$0.55 the potential to form intermediate TeO_{4+1} structures is depleted and real TeO_5 units occur. Figure 8 shows only one type of the corresponding TeO_{4+1} and TeO_5 units formed in the related crystal structures. Uniform types of polyhedral geometry are not identified. A great variety of TeO_5 units should exist in the glass structures where distances of 0.21 nm dominate (cf figures 4 and 8).

4.3. Comparison of RDFs of selected glasses with those of related crystal structures

The total $T_N(r)$ and $T_X(r)$ functions of the related crystal structures are calculated in the distance range of SRO and compared with the experimental $T(r)$ results of the samples with compositions close to those of the related crystalline compounds. The N_{ij} and r_{ij} parameters are taken from the crystal structures. Convolutions with the peak shape functions are made to simulate the termination effects of the Fourier transformations which exist in the experimental $T(r)$ data (cf section 3.2) [37, 38]. Peak widths Δr_{ij} are introduced to simulate glassy disorder and are adjusted to give best agreement of the peaks with those in the model functions. The weighting factors used in the calculations of the model $T(r)$ functions are taken from the glasses whose $T(r)$ data are used for comparison. Use of these factors avoids differences of peak heights which are only due to differences of atomic fractions.

The first comparisons are made for the polymorphs of TeO_2 [40–42] with the $T(r)$ data of glass tek08. On top of figure 9, comparisons are made with the $T(r)$ functions of glass tep02 which also shows the effects of a small $c(M_zO)$ fraction but with P_2O_5 instead of K_2O. Differences at 0.155 and 0.255 nm are due to P–O and O–O distances of the PO_4 units in the tep02 samples. Another difference is a small increase of the Te–O bond lengths for tep02. Since K_2O and P_2O_5 have quite different effects on TeO_n networks (section 4.1) possible changes in $T(r)$ for a glass of pure TeO_2 are expected in the limits of the $T(r)$ changes of tek08 and tep02 samples. The Te–O distances of the α-, β- and γ-forms agree with the experimental Te–O peaks (figure 9). Best agreement is obtained for β-TeO_2 whose $T_{TeO}(r)$ data possess smooth

behaviour with a constant contribution beyond 0.23 nm. On the other hand, the O–O peak which belongs to the edges of the TeO_n units is only well reproduced with the O–O distances of α-TeO_2. Small differences exist for the β-form. The TeO_4 of γ-TeO_2, however, possess strongly distorted O–Te–O angles which lead to O–O distances not being typical for v-TeO_2. Thus, the TeO_4 units of the tek08 glass show small changes of Te–O bond lengths if compared with α-TeO_2 but good agreement of the internal angles of the TeO_4 units with those of α-TeO_2.

The O–O peaks of the glasses tek08 and tep02 show no special features (except of a small contribution of edges of PO_4 tetrahedra at 0.252 nm for tep02). The N_{OO} numbers for both samples are ∼5 (tables 2 and 3) which number is expected for continuous networks of corner-connected TeO_4 tbps. Every oxygen atom in a Te_{ax}–O_{eq}–Te bridge has five first oxygen neighbours at ∼0.280 nm, two in the O_{ax} and three in the O_{eq} position (cf figure 9). The O–O distances with the O neighbours in 'weak' bonds are clearly longer than 0.28 nm. N_{OO} obtained from the experiments is a mean number and disorder in the connections of Te–O_{eq} and Te–O_{ax} bonds is expected for a glass. With increasing K_2O or P_2O_5 content the N_{OO} numbers of the glasses for the peak at 0.28 nm decrease due to disrupture of Te–O–Te bridges or replacement of Te by P positions.

From spectroscopic results of TeO_2 glass and crystals other authors [73] suggested most similarity with the structure of γ-TeO_2 [42]. Also recrystallization of v-TeO_2 starts with γ-TeO_2 [73]. The role of small P_2O_5 or K_2O contents of those glasses (tep02, tek08) which are used in the comparisons is not fully clear. But comparisons in [73] were also made with pure and doped TeO_2 glasses with no serious changes in the results. On the other hand, from consideration of the network structures of the three TeO_2 polymorphs it is suggested that the β-form of TeO_2 has a layer-like network structure also with edge-connections between the TeO_4 units. The γ-form has a 3D-network of corner-connected TeO_4 units but with the short Te–O bonds in chain orientation. Edge-connections and strong orientations of the units change the O–Te–O angles. Consequently, a network developed likewise in all three dimensions with preferably corner-connected TeO_4 tbps as in α-TeO_2 is suggested for v-TeO_2 but with some disorder in the Te–O_{ax} and Te–O_{eq} links and, possibly, with small fractions of TeO_{4+1} and TeO_{3+1} units.

The next comparisons are made for the $P_2Te_3O_{11}$ [31] and $P_2Te_4O_{13}$ [32] crystals. The groups in $P_2Te_3O_{11}$ are two PO_4 tetrahedra, two TeO_5 units and a TeO_{4+1} unit where all oxygens are forming bridges except of an O atom having two 'strong' and an additional 'medium' Te–O bond. The structure of this crystal is close to the behaviour of model D. The corresponding $T(r)$ functions (figure 10(a)) show several differences from the $T(r)$ of the glass tep27. Too many Te–O bonds have distances of 0.21 nm but there is a deficit of distances of 0.19 nm. The other crystal $P_2Te_4O_{13}$ has only TeO_{4+1} instead of the TeO_5 expected according to model D. One P–O bond of each PO_4 is not a member of a typical P–O–Te bridge but the corresponding oxygens possess two Te neighbours forming only 'medium' and 'weak' bonds. Thus, different from our model assumption the P=O double bond is partially localized. The corresponding $T(r)$ functions (figure 10(b)) show small differences from the $T(r)$ of the glass tep19. The model Te–O peak is a little too small and distances are especially missing at 0.22 nm. Both crystal structures show that P–O distances less than 0.29 nm do not occur except for the short P–O bonds, which assumption was made in the analysis of the Te–O and O–O correlations (section 3.4).

The two crystal structures show differences from model D (each O has two neighbours) in opposite directions. $P_2Te_4O_{13}$ [32] has two oxygens where second neighbours are only in 'medium' Te–O bonds while $P_2Te_3O_{11}$ [31] has one oxygen with a third neighbour in a 'medium' Te–O bond. The comparisons of figure 10 have shown that the Te–O peaks of the glasses are found between those of both crystal structures (cf also the N_{TeO} in figure 7). The

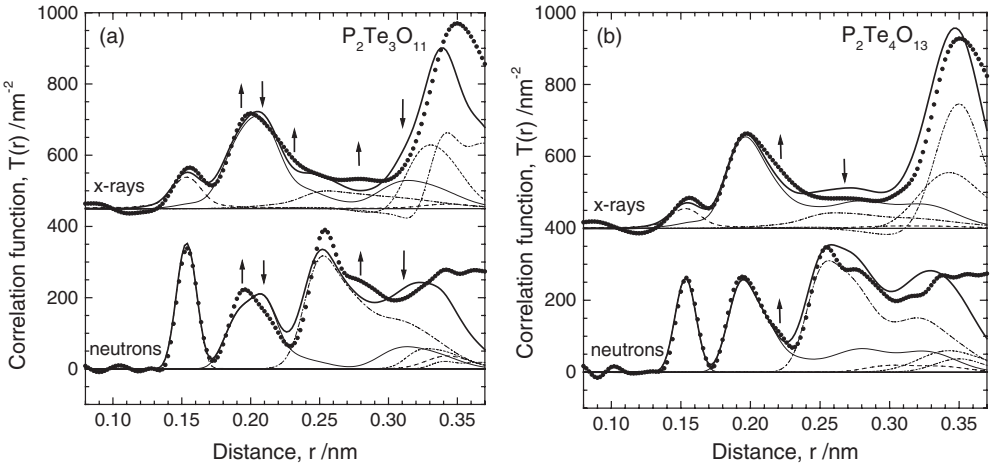

Figure 10. The experimental $T(r)$ functions (dots) of samples tep27 (a) and tep19 (b) compared with model $T(r)$ functions (thick solid lines) calculated by use of the SRO of crystals $P_2Te_3O_{11}$ [31] (a) and $P_2Te_4O_{13}$ [32] (b). Partial correlations: P–O—dashed lines; Te–O—thin solid lines; O–O—dash–dotted lines; Te–P—short dash lines; Te–Te—dash–double-dot lines. The vertical arrows indicate if downward, surfeit of distances; if upward, deficiency of distances of the model function in comparison with the experimental results.

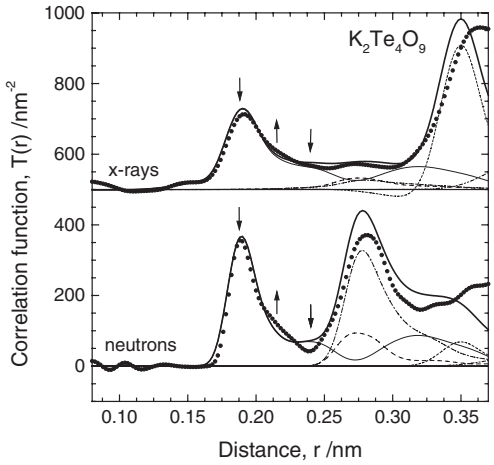

Figure 11. The experimental $T(r)$ functions (dots) of sample tek16 compared with model $T(r)$ functions (thick solid lines) calculated by use of the SRO of crystal $K_2Te_4O_9$ [34]. Partial correlations: Te–O—thin solid lines; O–O—dash–dotted lines; K–O—dashed lines; Te–Te—short dash lines; Te–K—dash–double-dot lines. The vertical arrows indicate if downward, surfeit of distances; if upward, deficiency of distances of the model function in comparison with the experimental results.

compositions of both crystalline compounds are close to $c(M_zO)$ of ∼0.55. Please remember that the shapes of the Te–O peaks of the glasses of these compositions indicate changes of the TeO_n units (section 4.2). It seems that the strong change from $P_2Te_4O_{13}$ with TeO_4 and TeO_{4+1} units to $P_2Te_3O_{11}$ with TeO_5 and TeO_{4+1} units is also reflected in the glass structures with a change from TeO_{4+1} to TeO_5 units. But for the glasses this change appears in a broad compositional interval. TeO_5 units appear already for glasses of P_2O_5 fractions less than that

of $P_2Te_4O_{13}$ and a greater number of TeO_{4+1} units still exists for P_2O_5 fractions greater than that of $P_2Te_3O_{11}$ (cf figure 7).

A last comparison is made for the $K_2Te_4O_9$ [34] crystal (figure 11) where the $T(r)$ data of sample tek16 are used. The $T(r)$ functions of tek16 show a surfeit of Te–O distances at ∼0.22 nm but deficit of Te–O distances at ∼0.19 and ∼0.24 nm. This difference might be due to the higher fraction of TeO_4 tbps instead of TeO_{3+1} units in the glass which is expected according to the different compositions of 16 and 20 mol% K_2O for glass and crystal. Thus, also for the K_2O–TeO_2 system it is shown that the transition to TeO_3 units should include the TeO_{3+1} units. A few additional oxygens have been found at 0.28 nm (table 2). The diffraction results are not sufficient to conclude the existence of oxygens at 0.32 nm which complete the highly distorted TeO_6 octahedra formed in the structure of the $K_2Te_4O_9$ [34] crystal.

4.4. The amphoteric character of TeO_2

The large ranges of glass formation of binary tellurite glasses with additions ranging from alkali oxide to phosphorus pentoxide [63] are due to the great variability of Te(IV) atoms forming different oxygen coordination polyhedra. Their LPEs prevent formation of stable polyhedra of high symmetry (high bond energy). The LPEs enable the Te sites to form links of quite different bond valency. The needs of other atomic partners can be satisfied properly. Addition of a great number of K^+ ions is accompanied by addition of a comparably small number of oxygen atoms. Formation of a maximum number of O_T with electron charges less than unity is advantageous for coordination of the K^+ ions. The O atom added with K_2O disruptures a Te–O–Te bridge between two TeO_4 tbps creating two O_T. The $TeO_4 \rightarrow TeO_3$ transition doubles the number of O_T with

$$2TeO_{4/2} + O^{2-} \rightarrow 2(TeO_{3/2}O)^- \rightarrow 2(TeO_{1/2}O_2)^-. \tag{5}$$

Writing $O_{n/2}$ means oxygen shared in bridges while full O are in terminal positions. The transitions seem to be more complicated if O atoms in 'medium' and 'weak' Te–O bonds are taken into account. These bonds allow the formation of various transitional groups. It is also emphasized that the large K^+ ions expand the network. A new medium-range order distance appears which is expressed as the first peak at ∼13 nm^{-1} in the $S_N(Q)$ factors or the prepeak in the $S_X(Q)$ factors (figure 3). This peak grows with increasing K_2O content. The small remaining number of network links limits glass formation in the K_2O–TeO_2 system.

A $TeO_4 \rightarrow TeO_3$ transition is still profitable for glasses with Al^{3+} and Ga^{3+} ions (figure 7). Certainly, the O_T form Te–O_T–M bridges in this case and are not shared between several M neighbours as needed for K^+ ions. Step by step, the $TeO_4 \rightarrow TeO_3$ transition is reduced if $M^{\nu+}$ ions of higher valency and smaller dimension are added. High numbers of O_T become disadvantageous. Also the second oxides show glass forming abilities which are expressed in the existence of the M–O–M bridges. As discussed before most M atoms are variable in forming mixtures of different MO_n polyhedra. This ability is useful because Te–O_{eq} and Te–O_{ax} bonds of TeO_4 tbps are not equivalent to each other (Te–O_{eq} is stronger than Te–O_{ax}) and need different bond partners. The bond valence in BO_4 or GeO_6 polyhedra is less than unity. Such bonds can be balanced either in bridges with strong Te–O_{eq} bonds or in sharing corners with two Te–O_{ax} bonds. These needs might be problematic with stiff SiO_4 units in the formation of a SiO_2–TeO_2 glass which is not known to be prepared so far though ternary TeO_2–B_2O_3–SiO_2 glasses exist [74]. From this point of view it is interesting that PO_4 tetrahedra are well incorporated in tellurite networks. Though the fraction of π-bonding in the P–O bonds of isolated PO_4 tetrahedra is distributed to all four bonds [71] its strength can be split according to the needs of the neighbouring TeO_n units. The addition of a small number of P^{5+} ions is

accompanied by the addition of a comparably great number of oxygen atoms. The response of Te(IV) atoms is an increase of N_{TeO} because P^{5+} ions require a small number (four) of oxygen neighbours but each with a great charge of ∼1.25 electrons. In the competition for the electron charge TeO_2 loses to P_2O_5 (tellurium acts as a Lewis base). P_2O_5 realizes its optimum structure: four-connected PO_4 units fixing 1.25 electrons in each P–O bond instead of three-connected PO_4 units with the fourth corner forming a P=O double bond. TeO_2 has to accept additional oxygen with deficit of electrons with

$$PO_{3/2}O + TeO_{4/2} \rightarrow (PO_{4/2})^{-} + (TeO_{5/2})^{+}. \tag{6}$$

The Te(IV) atoms seem not to resist this change too much. Anyway, strongly distorted TeO_6 octahedra are known in the structure of pure TeO_2 (glass and crystal, cf figure 8). Little alteration is needed. The units change to octahedra with the LPEs being sterically less effective. A greater number of 'strong' Te–O bonds appears, however, with greater bond lengths.

The changes of the effects of the LPE ($5s^2$ electrons) for Te^{4+} can be compared with the effects of the LPE ($6s^2$ electrons) for Pb^{2+} except that the greater Pb^{2+} ions have eight oxygen neighbours. A PbO_4 tbp as part of a strongly distorted PbO_8 polyhedron is formed in the structure of the $PbSiO_3$ crystal [75]. The oxygen neighbours of the longer Pb–O bonds have distances of ⩾0.30 nm. The structure of a PbV_2O_6 crystal [76] shows already a less distorted PbO_8 polyhedron. Finally, the distortions of PbO_8 polyhedra are lost in the structure of PbP_2O_6 [77] with the LPE not being sterically active. Here also the greater number of available oxygens forces the PbO_8 polyhedra to avoid distortions. The same change is detected for the Pb–O environments in the corresponding PbO–SiO_2, PbO–V_2O_5 and PbO–P_2O_5 glasses [78]. The Pb–O environments were found to depend on the species M of second oxide M_zO.

5. Conclusions

Three advantageous circumstances have been applied in a diffraction study of the SRO of tellurite glasses: results of neutron and x-ray diffraction experiments are combined (contrast variation). Both experiments were performed using high resolving power ($Q_{\max}$ of 400 or 280 nm^{-1} with neutrons from a spallation source or high-energy x-ray photons from a synchrotron). The P–O or K–O bond lengths of the P_2O_5–TeO_2 or K_2O–TeO_2 glasses do not interfere with the Te–O first-neighbour peaks. Moreover, first P–O distances except the short P–O bonds appear only beyond 0.29 nm. So the Te–O and O–O correlations are approximated by Gaussian fitting of the x-ray and neutron correlation functions up to lengths of 0.28 nm. In the case of K_2O–TeO_2 glasses reasonable assumptions are made for the K–O first-neighbour peaks at ∼0.275 nm.

Te–O and O–O coordination numbers of four and five are found for the glasses of compositions close to TeO_2 which indicates formation of a three-dimensional network of preferably corner-connected TeO_4 tpbs. The network groups are TeO_4 and TeO_3 units in K_2O–TeO_2 glasses and TeO_4 and TeO_5 units in P_2O_5–TeO_2 glasses. Additional Te–O neighbours are determined in an interval $0.23\ \mathrm{nm} < r < 0.29\ \mathrm{nm}$. For K_2O–TeO_2 glasses existence of TeO_{3+1} units is suggested. For the P_2O_5–TeO_2 glasses distorted TeO_6 polyhedra exist independent of the P_2O_5 content.

The unusual increase of the Te–O coordination number in P_2O_5–TeO_2 glasses is due to the strong preference of the PO_4 tetrahedra to form equivalent P–O bonds typical for orthophosphate $(PO_{4/2})^{-}$ units. The formation of TeO_{4+1} and TeO_5 units compensates for the surfeit of oxygen and deficiency of electron charge. The increase of the Te–O coordination state is realized by reduction of the steric effect of the LPE where with P_2O_5 additions a change from highly distorted TeO_6 octahedra in TeO_2 to less distorted TeO_6 with higher fraction of

Te–O distances in the range of 'strong' bonds occurs. In this process the number of Te–O distances of ∼0.21 nm exceeds those of ∼0.19 nm.

Acknowledgment

Financial support of the Deutsche Forschungsgemeinschaft (contract KR 1372/9-1) is gratefully acknowledged.

References

[1] Mazurin O V, Streltsina M V and Shvaiko-Shvaikovskaya T P 1985 *Handbook of Glass Data* Part B (Amsterdam: Elsevier)
Mazurin O V, Streltsina M V and Shvaiko-Shvaikovskaya T P 1991 *Handbook of Glass Data* Part D (Amsterdam: Elsevier)
Mazurin O V, Streltsina M V and Shvaiko-Shvaikovskaya T P 1993 *Handbook of Glass Data* Part E (Amsterdam: Elsevier)
[2] Bürger H, Fink K-G, Vogel W, Koshukharov V and Marinov M 1985 *Glastechnische Berichte* **58** 211
[3] Yano T, Fukumoto A and Watanabe A 1971 *J. Appl. Phys.* **42** 3674
[4] Kim S-H, Yoko T and Sakka S 1993 *J. Am. Ceram. Soc.* **76** 2486
[5] Dimitrov V and Komatsu T 1999 *J. Non-Cryst. Solids* **249** 160
[6] Kim S I and Yun S I 1994 *J. Lumin.* **60/61** 233
[7] Wand J S, Vogel E M and Snitzer E 1994 *Opt. Mater.* **3** 187
[8] Bürger H, Vogel W and Kozhukharov 1985 *Infrared Phys.* **25** 395
[9] Bürger H, Gugov I, Grünke U, Kraus J and Manzanares-Taylor E 2002 *Glass Sci. Technol.* **75C** 261
[10] Zemann J 1971 *Monatsh. Chem.* **102** 1209
[11] Bart J C J and Giordano N 1979 *Gazzetta Chim. Italiana* **109** 73
[12] Bürger H and Gugov I 1998 *Glass Sci. Technol.* **71C** 321
[13] Tatsumisago M, Minami T, Kowada Y and Adachi H 1994 *Phys. Chem. Glasses* **35** 89
[14] Lee S K, Tatsumisago M and Minami T 1994 *Phys. Chem. Glasses* **35** 226
[15] Bürger H 1990 *Thesis* Friedrich-Schiller-Universität Jena
[16] McLaughlin J C, Tagg S L and Zwanziger J W 2001 *J. Phys. Chem.* B **105** 67
[17] Iwadate Y, Mori T, Hattori T, Nishiyama S, Fukushima K, Umesaki N, Akagi R, Handa K, Ohtori N, Nakazawa T and Iwamoto A 2000 *J. Alloys Compounds* **311** 153
[18] Akagi R, Handa K, Ohtori N, Hannon A C, Tatsumisago M and Umesaki N 1999 *J. Non-Cryst. Solids* **256/257** 111
[19] Nishida T, Yamada M, Hiroshi I and Takashima Y 1990 *J. Mater. Sci.* **25** 3546
[20] Sekiya T, Mochida N, Ohtsuka A and Tonokawa M 1992 *J. Non-Cryst. Solids* **144** 128
[21] Kieffer J, Masnik J E, Nickolayev O and Bass J D 1998 *Phys. Rev.* B **58** 694
[22] Sakida S, Hayakawa S and Yoko T 1999 *J. Non-Cryst. Solids* **243** 13
[23] Neov S, Ishmaev S and Kozhukharov 1995 *J. Non-Cryst. Solids* **192/193** 61
[24] Soper A K and Buchanan P 2004 private communication
Hannon A C 2004 http://www.isis.rl.ac.uk/disordered/manuals/gudrun/gudrun_gem.htm
[25] Faber T E and Ziman J M 1965 *Phil. Mag.* **11** 153
[26] Poulsen H F, Neuefeind J, Neumann H-B, Schneider J R and Zeidler M D 1995 *J. Non-Cryst. Solids* **188** 63
[27] Maslen E N, Fox A G and O'Keefe M A 1992 *International Tables for Crystallography* vol C, ed A J C Wilson (Dordrecht: Kluwer) p 476
[28] Hubbell J H, Veigele Wm J, Briggs E A, Brown R T, Cromer D T and Howerton R J 1975 *J. Phys. Chem. Ref. Data* **4** 471
[29] Waseda Y 1980 *The Structure of Non-Crystalline Materials* (New York: McGraw-Hill) p 11
[30] Lorch E A 1969 *J. Phys. C: Solid State Phys.* **2** 229
[31] Mayer H and Weil M 2003 *Z. Anorg. Allg. Chem.* **629** 1068
[32] Mayer H and Pupp G 1977 *Z. Kristallogr. Kristallgeom. Kristallphys. Kristallchem.* **145** 321
[33] Hoppe U, Walter G, Stachel D and Hannon A C 1996 *Z. Naturf.* a **51** 179
[34] Becker C R, Tagg S L, Huffman J C and Zwanziger J W 1997 *Inorg. Chem.* **36** 5559
[35] Hoppe U, Yousef E, Rüssel C, Neuefeind J and Hannon A C 2002 *Solid State Commun.* **123** 273
[36] Hoppe U, Yousef E, Rüssel C, Neuefeind J and Hannon A C 2004 *J. Phys.: Condens. Matter* **16** 1645

[37] Mozzi R L and Warren B E 1969 *J. Appl. Crystallogr.* **2** 164
[38] Leadbetter A J and Wright A C 1972 *J. Non-Cryst. Solids* **7** 23
[39] Marquardt D 1963 *SIAM J. Appl. Math.* **11** 431
[40] Thomas P A 1988 *J. Phys. C: Solid State Phys.* **21** 4611
[41] Beyer H 1967 *Z. Kristallogr.* **124** 228
[42] Champarnaud-Mesjard J-C, Blanchandin S, Thomas P, Mirgorodsky A P, Merle-Méjean T and Frit B 2000 *J. Phys. Chem. Solids* **61** 1499
[43] Philippot E 1981 *J. Solid State Chem.* **38** 26
[44] Hoppe U, Walter G, Kranold R and Stachel D 2000 *J. Non-Cryst. Solids* **263/264** 29
[45] Walter G, Hoppe U, Vogel J, Carl G and Hartmann P 2004 *J. Non-Cryst. Solids* **333** 252
[46] Karakassides M A, Saranti A and Koutselas I 2004 *J. Non-Cryst. Solids* **347** 69
[47] Ueno M and Suzuki K 1983 *Res. Rep. Lab. Nucl. Sci. Tohoku Univ.* **16** 49
[48] Suzuki K 1987 *J. Non-Cryst. Solids* **95/96** 15
[49] Niida H, Uchino T, Jin J, Kim S-H, Fukunaga T and Yoko T 2001 *J. Chem. Phys.* **114** 459
[50] Meunier G and Galy J 1971 *Acta Crystallogr.* B **27** 602
[51] Loopstra B O and Goubitz K 1986 *Acta Crystallogr.* C **42** 520
[52] Andersen L, Langer V, Stroemberg A and Stroemberg D 1989 *Acta Crystallogr.* B **45** 344
[53] Hanke K 1966 *Naturwissenschaften* **53** 273
[54] Blanchandin S, Champarnaud-Mesjard J C, Thomas P and Frit B 2000 *J. Alloys Compounds* **306** 175
[55] Galy J and Lindquist O 1979 *J. Solid State Chem.* **27** 279
[56] Darriet J and Galy J 1973 *Cryst. Struct. Commun.* **2** 237
[57] Brown I D 1974 *J. Solid State Chem.* **11** 214
[58] Himei Y, Osaka A, Nanba T and Miura Y 1994 *J. Non-Cryst. Solids* **177** 164
[59] Sakida S, Hayakawa S and Yoko T 1999 *J. Ceram. Soc. Japan* **107** 395
[60] Sakida S, Hayakawa S and Yoko T 2001 *J. Am. Ceram. Soc.* **84** 836
[61] Charton P and Armand P 2004 *J. Non-Cryst. Solids* **333** 307
[62] Sakida S, Hayakawa S and Yoko T 2000 *J. Phys.: Condens. Matter* **12** 2579
[63] Vogel W 1992 *Glass Chemistry* 2nd English edn (Berlin: Springer) p 167
[64] Kashchieva E P and Dimitriev Y B 1997 *J. Am. Ceram. Soc.* **80** 1588
[65] Göring R, Bürger H, Nass H and Schnabel B 1981 *Phys. Status Solidi* a **68** K29
[66] Osaka A, Qiu J R, Miura Y and Yao J W 1995 *J. Non-Cryst. Solids* **191** 339
[67] Osaka A, Jianrong Q, Nanba T, Takada J and Miura Y 1992 *J. Non-Cryst. Solids* **142** 81
[68] Galeener F L and Mikkelsen J C 1979 *Solid State Commun.* **30** 505
[69] Hoppe U, Walter G, Barz A, Stachel D and Hannon A C 1998 *J. Phys.: Condens. Matter* **10** 261
[70] Van Wazer J R 1958 *Phosphorus and its Compounds* vol 1 (New York: Interscience) p 717 ff
[71] Hoppe U 1996 *J. Non-Cryst. Solids* **195** 138
[72] Brow R K 2000 *J. Non-Cryst. Solids* **263/264** 1
[73] Noguera O, Merle-Méjean T, Mirgorodsky A P, Smirnov M B, Thomas P and Champarnaud-Mesjard J-C 2003 *J. Non-Cryst. Solids* **330** 50
[74] Dimitriev Y B, Bursukova M A, Kashchieva E P and Gotchev E P 1997 *J. Mater. Sci. Lett.* **16** 1622
[75] Boucher M L and Peacor D R 1968 *Z. Kristallgr. Kristallgeom. Kristallphys. Kristallchem.* **126** 98
[76] Calestani G, Andreetti G D, Montenero A, Bettinelli M and Rebizaut J 1985 *Acta Crystallogr.* C **41** 179
[77] Jost K H 1964 *Acta Crystallogr.* **17** 1539
[78] Hoppe U, Kranold R, Ghosh A, Landron C, Neuefeind J and Jóvári P 2003 *J. Non-Cryst. Solids* **328** 146